MODELING TIDAL DYNAMICS IN A MANGROVE CREEK CATCHMENT IN DELFT3D

Erik Horstman[1,2], Marjolein Dohmen-Janssen[1], Suzanne Hulscher[1]

Abstract

Modeling tidal dynamics in mangroves is of great use in studying the effects of changes in e.g. vegetation cover or tidal forcing. Process based models, taking into account vegetation drag and turbulence, have not yet been applied to study tidal dynamics in mangrove forests. We compare three different model representations of vegetation in Delft3D-FLOW for their accuracy and efficiency in modeling tidal dynamics in a schematized mangrove creek catchment: (i) a three-dimensional model taking into account vegetation induced momentum loss and turbulence generation and dissipation (3D-DPM); (ii) a two-dimensional depth-averaged model taking into account the vegetation induced momentum loss (2DH-DPM); and (iii) a two-dimensional depth-averaged model applying an adjusted bed roughness and an artificial term for momentum loss (2DH-Baptist). All models predict flow velocities, suspended sediment concentrations and sediment deposition rates of the same order of magnitude as observed in the field. Compared to the 3D-DPM model which resolves all vegetation impacts, the 2D-DPM model predicts resembling hydro- and sediment dynamics, but at a significantly increased computational efficiency. This efficiency is useful when modeling real mangrove wetlands, requiring high grid resolution due to great spatial topographic variability. Increased model efficiency also enhances the feasibility of sensitivity analyses of the short- and long-term development of mangroves under changing conditions.

Key words: mangroves, tidal dynamics, hydrodynamics, sediment dynamics, model comparison, Delft3D

1. Introduction

Mangroves thrive in sheltered intertidal areas of (sub-)tropical coastlines. Because of their position at the interface between land and sea, mangroves play a pivotal role in local hydro- and sediment dynamics. Field studies have shown that mangroves impact the magnitude and direction of tidal and riverine water flows (e.g. Kobashi and Mazda, 2005) and enhance sediment deposition rates (e.g. Van Santen et al., 2007). These field studies are typically based on local case studies and consequently often comprise just a limited range of environmental parameters (e.g. vegetation cover, elevation) and hydrodynamic exposure (e.g. tidal amplitude, waves). With these limitations of field data, numerical models are indispensable to analyze the effects of these parameters on mangrove hydro- and sediment dynamics (Temmerman et al., 2005).

Previous modeling studies into mangroves' tidal scale hydrodynamics were mainly concerned with creek-forest interactions and the consequent tidal asymmetry in mangrove creek systems (e.g. Mazda et al., 1995). This focus allows for simple parameterizations of the hydrodynamic impacts of mangrove vegetation. So far, analytical and numerical studies applied one- and two-dimensional modeling approaches, representing vegetation by an adjusted roughness parameter, and a largely simplified topography (Wolanski et al., 1990; Mazda et al., 1995; Furukawa et al., 1997). Studies into tidal-scale hydrodynamics within mangroves require a more advanced approach of modeling the effect of these trees on hydrodynamics. Hereto, Mazda et al. (2005) and Kobashi & Mazda (2005) introduced vegetation induced drag forces into the momentum equation, related directly to a vegetation density parameter. This approach was extended by Wu et al. (2001), who included both vegetation induced drag and the blockage effect by the vegetation. However, none of these models take into account the depth dependency of the vegetation characteristics or local topography. Hence simulated (depth-averaged) flow patterns might not represent field conditions.

Modeling tidal-scale sediment dynamics in mangroves has been initiated by Wolanski et al. (1999). They extended a two-dimensional model for the prediction of suspended sediment transport fluxes in an

estuary. Wolanski et al. (1999) implemented parameterizations for the distribution of sediments in the smaller creeks and the adjoining mangroves, which were beyond the model's resolution. No further attempts of modeling short-term sediment dynamics in mangroves are known, reflecting the fact that only a few field studies are available measuring both hydrodynamics and sediment transport and/or deposition along transects in mangroves (Furukawa et al., 1997; Vo-Luong and Massel, 2006; Van Santen et al., 2007).

Recently, a three-dimensional process-based model in Delft3D-FLOW was applied to simulate tidal dynamics in salt marshes (Temmerman et al., 2005). Such a process-based numerical model for simulating tidal-scale hydro- and sediment dynamics in mangroves is missing yet. Due to the vast extent of mangrove creek catchments and the great spatial variability of their bathymetry, vegetation cover and sediment characteristics, calculation grids will need to cover a large area at a high resolution, increasing computational demands. This raises questions on the suitability of two-dimensional depth-averaged (2DH) models instead of the – computationally expensive – three-dimensional (3D) model for salt marshes.

Our aim is to compare simplified 2DH approaches for modeling vegetation dynamics in Delft3D-FLOW to the previously deployed 3D process-based numerical model. These models should be suited to simulate tidal-scale hydro- and sediment dynamics in coastal mangroves and to analyze the sensitivity of these processes to changing parameter settings. The models will be validated against field data obtained in mangrove forests in Thailand. A schematized mangrove area is studied to reduce the model's run time.

This paper first introduces Delft3D and the different ways in which vegetation effects are taken into account in its 3D and 2DH models. This section also presents field data that are used for model validation and the schematized study area for which the models are run. Section 3 presents the results of the different models, before and after calibration, including an analysis of the model sensitivity to uncertain input parameters. Our findings are discussed in section 4 and our main conclusions are summarized in section 5.

2. Methods

2.1. *Delft3D model resolving 3D flow and turbulence effects of vegetation*

The Delft3D-FLOW software simulates flow hydrodynamics, sediment dynamics and morphological processes in shallow water environments. Delft3D-FLOW solves the two-dimensional (depth-averaged) or three-dimensional unsteady shallow water equations, applying the hydrostatic pressure assumption. Transport and deposition of sediments is computed simultaneously with the hydrodynamics, creating direct feedback between hydro- and morphodynamics (Deltares, 2012). Delft3D-FLOW is suited with a flooding and drying algorithm. Grid cells are activated when water levels exceed a flooding threshold, while grid cells are de-activated when local water levels drop below half this threshold (Deltares, 2012).

Recent efforts to better understand the effect of plants on shallow water dynamics have led to new modules in Delft3D-FLOW simulating additional vegetation resistance (e.g. Baptist, 2005). Uittenbogaard (2003) extended the one-dimensional vertical (1DV) momentum equation and turbulence closures to account for the contribution of vegetation elements, represented as a collection of rigid vertical cylinders. This was implemented in Delft3D-FLOW through the directional point model (DPM). 1DV simulations with the DPM have been validated successfully against experimental flume data (Uittenbogaard, 2003; Baptist, 2005). The 3D implementation of this DPM vegetation representation has been calibrated and validated successfully for salt-marsh vegetation (Temmerman et al., 2005; Bouma et al., 2007).

In the DPM model, the depth-dependent contribution of the vegetation in the momentum equation is induced by the vegetation induced friction force (*F*):

$$F(z) = \frac{1}{2} \rho_w C_D n(z) D(z) |u(z)| u(z)$$ (1)

Wherein ρ_w is the water density [kg/m^3]; C_D represents the plant resistance coefficient [-]; n indicates the number of plant elements per unit area [m^{-2}] with diameter D [m]; and $u(z)$ for the horizontal velocity profile [m/s]. The number and diameter of the vegetation elements can be depth-dependent.

Additionally, the DPM model explicitly accounts for the obstruction of momentum and turbulence exchange due to the area taken by the vegetation. The solidity A_p [-] of the vegetation is defined as:

$$A_p(z) = \frac{1}{4} \pi D(z)^2 n(z) \tag{2}$$

Hence, $1-A_p$ is a measure for the vegetation porosity. Changes of fluxes due to (changes in) the vegetation's porosity are mostly disregarded in the present model, being developed initially for 1DV simulations. Yet, vertical momentum exchange is considered to depend significantly on vegetation porosity (Baptist, 2005):

$$\rho_0 \frac{\partial u(z)}{\partial t} + \frac{\partial p}{\partial x} = \frac{\rho_0}{1 - A_p(z)} \frac{\partial}{\partial z}\left(\left(1 - A_p(z)\right)\left(v + v_T(z)\right)\frac{\partial u(z)}{\partial z} \right) - \frac{F(z)}{1 - A_p(z)} \tag{3}$$

Wherein $\partial p/\partial x$ represents the horizontal pressure gradient [N/m³]; v is the kinematic viscosity of water [m²/s]; and v_T is the eddy viscosity [m²/s]. The eddy viscosity is calculated with a k-ε turbulence closure. These closures, including vegetation effects, are presented by Uittenbogaard (2003). Subsequently, suspended sediment transport is calculated by an advection-diffusion equation (Deltares, 2012):

$$\frac{\partial c}{\partial t} + \frac{\partial uc}{\partial x} + \frac{\partial vc}{\partial y} + \frac{\partial (w - w_s)c}{\partial z} = \frac{\partial}{\partial x}\left(D_H \frac{\partial c}{\partial x} \right) + \frac{\partial}{\partial y}\left(D_H \frac{\partial c}{\partial y} \right) + \frac{\partial}{\partial z}\left(D_V \frac{\partial c}{\partial z} \right) \tag{4}$$

Where c represents the suspended sediment concentration [kg/m³]; u, v and w are the velocity components in x, y and z directions respectively [m/s]; w_s is the settling velocity of the sediment [m/s]; and D_H and D_V represent the horizontal and vertical eddy diffusivity [m²/s]. For cohesive sediments, erosion (E_r) and deposition rates (D_r) [kg/m²/s] are calculated with the Partheniades-Krone formulations :

$$E_r = M\left(\frac{\tau_b}{\tau_{cr,e}} - 1 \right) \qquad \text{for } \tau_b > \tau_{cr,e} \quad \left(\text{else } E_r = 0 \right) \tag{5}$$

$$D_r = w_s c_b\left(1 - \frac{\tau_b}{\tau_{cr,d}} \right) \qquad \text{for } \tau_b < \tau_{cr,d} \quad \left(\text{else } D_r = 0 \right) \tag{6}$$

Wherein M is the erosion parameter [kg/m²/s]; τ_b is the bed shear stress [N/m²]; $\tau_{cr,e}$ is the critical bed shear stress for the initiation of erosion [N/m²]; c_b is the near-bed sediment concentration [kg/m³]; and $\tau_{cr,d}$ is the critical bed shear stress for deposition [N/m²]. Finally, the net deposition ND [kg/m²] is calculated by discounting the erosion and deposition rates and multiplying this net deposition rate by the time step.

2.2. Vegetation in 2DH simulations with Delft3D

Alternatively, the impacts of vegetation on hydro- and sediment dynamics can be simulated in a depth-averaged (2DH) mode. Two 2DH vegetation representations are available in Delft3D-FLOW: a direct method with the DPM, and an indirect approximation based on an artificial Chézy roughness value. The direct method only takes into account the additional momentum generated by the vegetation induced friction force F (eq.(1)), now calculated with the depth-averaged horizontal velocity $\bar{u}$ [m/s]. Changes in vertical vegetation geometry as well as changes to vertical fluxes in the momentum equation (eq.(3)) cannot be taken into account. The 3D turbulence closures are not resolved in this 2DH approach either.

The indirect method builds upon Baptist et al.'s (2007) analytical formulation for the contribution of vegetation resistance to the total roughness in water flowing through vegetation. They obtained a simplified but accurate version of their analytical formula for the representative Chézy roughness coefficient (C_r):

$$C_r = \sqrt{ \frac{1}{\dfrac{1}{C_b^2} + \dfrac{C_D n D h_v}{2g}} } + \frac{\sqrt{g}}{\kappa} \ln\left(\frac{h}{h_v} \right) \tag{7}$$

Where C_b is the (alluvial) bed roughness coefficient [m$^{1/2}$/s]; h_v and h represent the vegetation height [m] and total water depth [m]; and κ is Von Kármán's constant [-]. As this increased bed roughness induces greater bed shear stresses, it gives rise to a physically unrealistic increase in sediment transport. Therefore, in Delft3D-FLOW, the total roughness is split in two separate terms in the momentum equation representing the bed roughness and the vegetation induced resistance, respectively (Deltares, 2012):

$$gi - \frac{g\bar{u}^2}{C^2 h} - \lambda \bar{u}^2 = 0 \tag{8}$$

$$C = C_b + \frac{\sqrt{g}}{\kappa} \ln\left(\frac{h}{h_v}\right)\sqrt{1 + \frac{C_D n D h_v C_b^2}{2g}} \tag{9}$$

$$\lambda = \frac{1}{2} C_D n D \frac{h_v}{h} \frac{C_b^2}{C^2} \tag{10}$$

Where C [m$^{1/2}$/s] represents the adjusted bed roughness and λ is the vegetation induced flow resistance parameter. Independent of the method for simulating vegetation effects on the hydrodynamics, suspended sediment transport is calculated through a reduced advection-diffusion equation discarding vertical components (i.e. the last terms at the left and right hand sides of eq.(4)). The subsequent calculation of erosion and deposition rates resembles the 3D approach (eq.(5) and eq.(6)), except that the near-bed sediment concentration c_b now equals the depth-averaged sediment concentration.

2.3. *Field data for model validation*

We collected data during a field campaign in Trang province, Thailand, from November 2010 to May 2011 (Horstman et al., subm.). The study site that is discussed in this paper consists of a characteristic 'elevated' mangrove forest, fronted by a cliff and incised by a complex network of branching creeks (Figure 1). This site is located at the east bank of the Mae Nam Trang, about 6 km upstream of the open sea, in the estuary where the Mae Nam Trang and the Khlong Palian merge.

The study area is covered by a monitoring grid of 24 spatially distributed points. Obtained data consists of high-resolution bathymetry, vegetation description, water levels, flow velocities, suspended sediment concentrations (SSCs), sediment deposition rates and sediment characteristics. The bathymetry of the study area is shown in Figure 1. The topography of the center of the study area shows scattered mud lobster mounds. Vegetation throughout the area is quite dense and shows some zonation. *Rhizophora* trees – with the typical stilt roots (Figure 1) – form the dominant vegetation type (Horstman et al., subm.).

This paper focusses on hydro- and sediment dynamics at two characteristic locations (Figure 1): CN located within the main creek in the northern part of the study area and FC in the middle of the study area about 60 m from the main creek. Water depths, flow velocities, flow directions and suspended sediment concentrations (SSCs) are plotted for both points, during an entire spring-neap tidal cycle, in Figure 2. Sediment deposition rates observed throughout the area are presented in Figure 1. These deposition data have been collected repeatedly during four spring-neap tidal cycles.
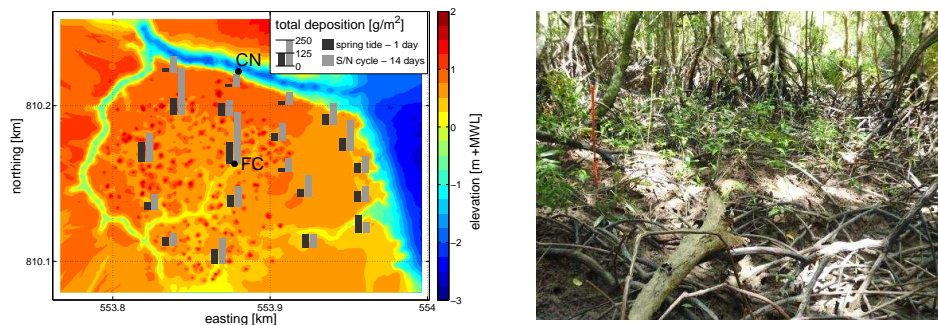

Figure 1. Left: bathymetry of the field site and locations of CN and FC (MWL=Mean Water Level). Right: vegetation in the surroundings of FC (the red stake is 1 m high).
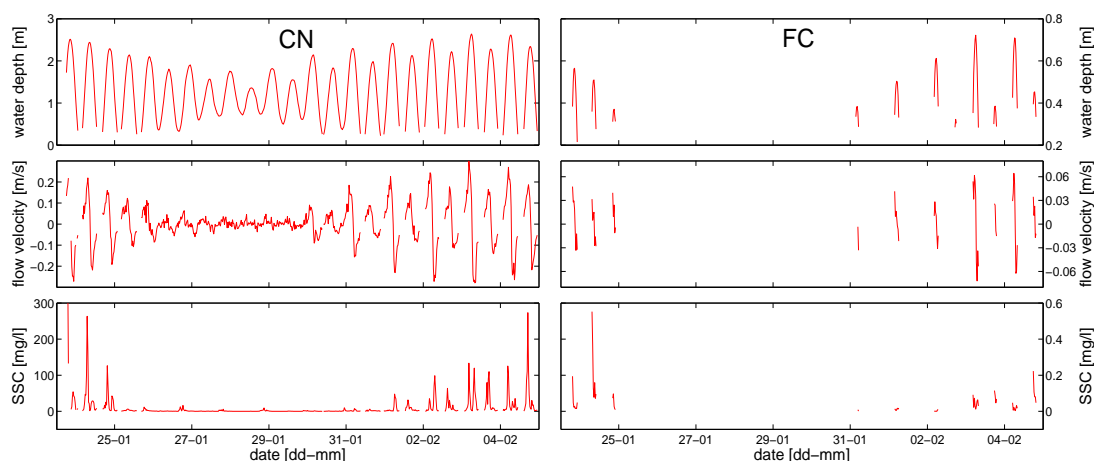
Figure 2. Water depths, flow velocities and SSCs at 7 cm above the bed at CN (left) and FC (right).

2.4. *Schematized study area for model comparison*

For convenient model comparisons, simulations in this paper are run for a schematized study area (Figure 3) with characteristic dimensions from the field site. The main creek in the field site is ~10-15 m wide and narrows down towards the end. The creek length estimated from satellite imagery is ~1 km (extending to the northwest in Figure 1) and feeds a mangrove area of ~0.5x0.5 km^2. Hence the swamp-to-creek ratio is 30($\pm$10), falling well within the 2.1-44 range found for a number of mangrove areas by Mazda et al. (1995).

The study area is schematized to a rectangular basin with a straight creek (c.f. Mazda et al., 1995; Wu et al., 2001). To avoid imposing additional boundary conditions, the forest floor is assumed to slope to a supratidal level of 2.0 m +MWL. The horizontal dimensions of the schematized area exceed the dimensions of the field site due to the combination of the elevated boundaries, the applied forest bed slope of 3.3:1000 (in the field slopes were 1:1000-5:1000) and the straightening of the creek. In order to maintain the characteristic elevations observed within and along the creek (creek's bed level starting at -2.0 m +MWL and banks at 0.5 m +MWL) while also complying with the swamp-to-creek ratio, the schematized creek's width was increased to 40 m. The widening of the upstream end of the creek is implemented to prevent for strong velocity increases due to the greater swamp-to-creek ratio in this part of the study area.

Model results presented in this paper are for positions within the creek and 70 m into the forest (CR and FO respectively; Figure 3), resembling the monitoring locations of the presented field data (Figure 1).

2.5. *Model parameters*

Parameter settings for the tidal climate, sediment conditions and vegetation characteristics are based on the field observations and are summarized in Table 1. Boundary conditions for tides and SSC are imposed
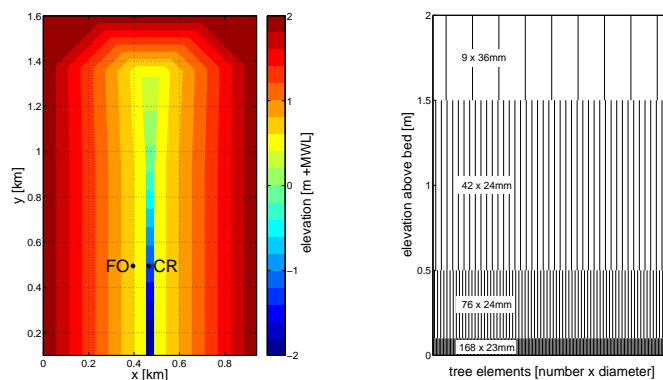

Figure 3. Bathymetry of the schematized study area with monitoring locations in the FOrest and CReek (left) and the measured geometry of the root system of a single *Rhizophora* tree (right).

at the seaside boundary of the model. The SSC boundary condition is based on measurements on the estuarine mudflat in front of the field site. The bed material, a cohesive sandy mud, contains 49($\pm$9)% silts and D_{50}=66.5($\pm$20) μm (ranges represent spatial heterogeneity (Horstman, 2012)). Although this grain size is at the upper limit of the silt range, the substrate is cohesive by its high content of silt and organic matter (8-19%). Sediment dynamics in the field are dominated by suspended transport and are modeled as such.

Vegetation characteristics were mapped intensively in mangrove sites surrounding the study area. One of these plots was assumed to resemble the vegetation within the study area. Figure 3 shows the measured geometry of the roots of one average *Rhizophora* tree. Vegetation characteristics are applied uniformly throughout the schematized area. For the 2DH models, only one layer of this geometry could be deployed.

Based on the sediment characteristics of the field site, ranges are calculated for bed roughness, critical bed shear stress and sediment settling velocity (Table 1). Initial settings for the model runs are summarized in Table 1 as well. The alluvial bed roughness was assumed uniformly at n=0.02 (Manning), as in previous studies (e.g. Wolanski et al., 1990; Furukawa et al., 1997). The critical bed shear stress was initially set at the mean value obtained from the sediment data. To avoid complex morphodynamics such as consolidation and bank erosion (Fagherazzi et al., 2012), a fixed bed is applied. Consequently, only sediments that are deposited during the model run can be eroded.

The model was run on a rather fine, squared grid with a 10 m mesh size, requiring a 6 s time step for stable model runs. The 3D model deploys 10 vertical (sigma-)layers, each covering 10% of the local water depth. The threshold depth for inundation of grid cells was set to 0.05 m. Standard values of the horizontal background viscosity and diffusivity (i.e. regular calibration parameters) were lowered due to the small mesh size of the grid: v_H = 0.1 m²/s (instead of 1.0 m²/s) and D_H = 1.0 m²/s (instead of 10 m²/s) respectively.

3. Model comparison, sensitivity and calibration

3.1. *Tidal flow velocities and flow routing*

Figure 4 shows the simulated depth-averaged flow velocities for one tidal cycle when the models are run for the parameters from Table 1. Flow velocities in the creek and in the forest compare well for the three models. Two reference runs are included: a 2DH model representing the vegetation resistance by an increased bed roughness n=0.125 (2DH-Manning); and a 2DH model with no vegetation (Figure 4). The 'Manning' vegetation representation results in higher flow velocities within the creek and lower velocities in the forest. Without vegetation, peak velocities within the forest are twice as high as with vegetation, while creek flow velocities are somewhat lower since more water is funneled over the bare intertidal flats.

Flow velocities predicted by the 3D-DPM model and 2DH-DPM and -Baptist models compare well with the field data. Predicted depth-averaged flow velocities within the forest are of $O(10^{-2})$ m/s, as are the velocities observed in the field (Figure 2). Within-creek depth-averaged flow velocities predicted by these models are an order of magnitude larger ($O(10^{-1})$ m/s) ranging up to 0.7 m/s. Within-creek velocities

Table 1: Characteristic parameter values as observed in the field (see: Horstman, 2012; Horstman et al., subm.) and the values applied in the 3D-DPM and 2DH-DPM and -Baptist models (n.a.=not available).

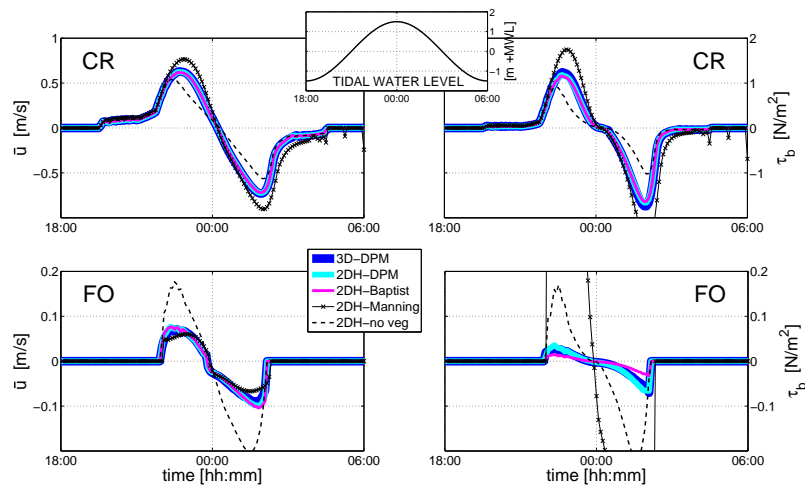| Parameter	Field	3D-DPM	2DH-DPM/Baptist
Tidal period T_T [hr]	12.25	12	12
Tidal amplitude A_T [m]	0.25<A_t<1.95	1.5	1.5
SSC [mg/l]	$O(10)$	40	40
Tree density [trees/m²]	0.07-0.20	0.15	0.15
Tree geometry	Figure 3	Figure 3	Figure 3, 2nd layer
C_b [Manning's n]	0.01-0.04	0.02	0.02
τ_{cr} [N/m²]	0.10-0.15	0.13	0.13
w_s [m/s]	$1 \cdot 10^{-3}$-$7 \cdot 10^{-3}$	$4 \cdot 10^{-3}$	$4 \cdot 10^{-3}$
M [kg/m²/s]	n.a.	10^{-2}	10^{-2}
v_H [m²/s]	n.a.	0.1	0.1
D_H [m²/s]	n.a.	1.0	1.0

Figure 4. Simulated depth-averaged flow velocities and bed shear stresses for points located within the creek (CR) and in the forest (FO). Results show the effect of different vegetation representations (DPM, Baptist, Manning) and different model settings (3D with depth-variable vegetation or 2DH with depth-uniform vegetation). For reference, the results of a run without vegetation are included (no veg).

in the field are also of $O(10^{-1})$ m/s, never exceeding 0.3 m/s at 7 cm above the bed (Figure 2). It was observed in the field that depth-averaged flow velocities exceed measurements at 7 cm above the bed, as flow velocities were found to increase non-logarithmically above the bed up to 1.5-2.8 times the velocity at 7 cm above the bed (Horstman et al., subm.).

Simulated flow routing patterns throughout the study area (Figure 5) indicate the relevance of creek flow (i.e. inflow from the estuary via the creek) over sheet flow (i.e. inflow from the estuary directly into the forest) in filling and emptying the tidal prism of the mangroves. On the initial and final stages of the mangroves' flooding, flow directions are mainly directed from/to the creek. At high water, flow directions throughout the forest are directed more parallel to the creek. Noteworthy is the flow routing at high tide: while the creek still transports water into (flooding) the area, sheet flow through the forest is discharging (ebbing) yet. This delayed flow reversal in the creek was also observed in the field (Horstman et al., subm.).

3.2. *Bed shear stresses*

Figure 4 shows that predicted bed shear stresses within the creek are comparable for each of the models. The simulations with increased Manning roughness and without vegetation show bed shear stresses in accordance with the trends in predicted depth-averaged flow velocities.

Within the forest, the simulation results diverge substantially. Figure 4 shows that the bed shear stresses predicted by the 2DH-DPM model represent the results of the 3D-DPM model. On the contrary, the 2DH-
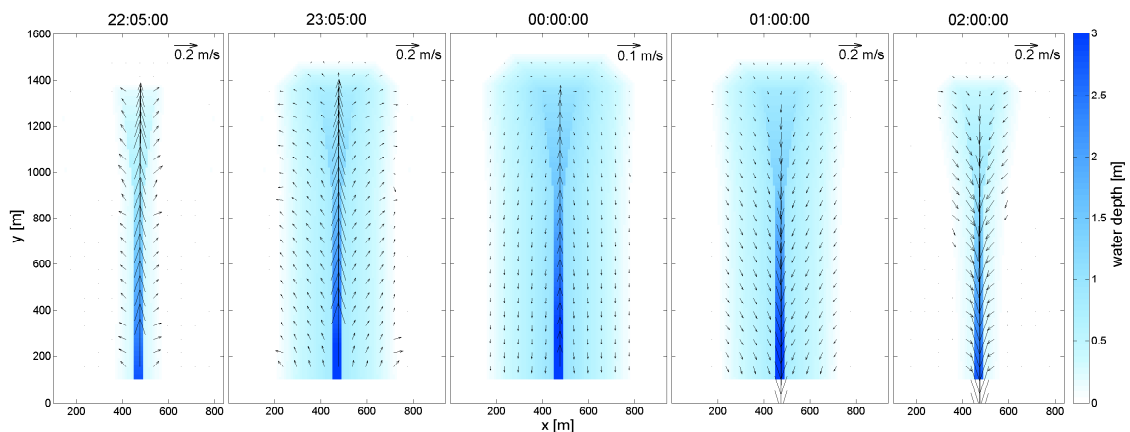

Figure 5. Simulated flow routing through the study area during a single tidal cycle (2DH-DPM model).

Baptist approach underpredicts the bed shear stresses within the forest. This can be related to the artificial separation of the bed and vegetation related resistance terms in eq.(8)-(10). Apparently, the vegetation resistance parameter λ assigns too much momentum loss to the vegetation resistance and hence reduces the adjusted bed resistance term in the momentum equation, resulting in reduced bed shear stresses.

The bed shear stresses calculated from the reference runs are much greater. Without vegetation, bed shear stresses experienced within the forest are up to 4-6 times greater than with mangroves surrounding the creek. The model run with increased Manning bed roughness, representing all resistance induced by both the bed and the vegetation, predicts bed shear stresses up to 15-25 times greater than the 3D-DPM run.

3.3. *Suspended sediment concentrations and deposition rates*

Within the creek, SSCs simulated by the 3D- and 2DH-DPM models are resembling, while the 2DH-Baptist run shows a slight underprediction of the SSC on ebb tide compared to the 3D-DPM run (Figure 6). Within the forest, the predicted SSCs differ substantially. The maximum SSC during flood tide is ~7 times larger for the 2DH-DPM model than for the 3D-DPM model.

Model results compare well with field data for within-creek SSCs, especially on flood tide. Field observations of within-creek SSCs are of $O(10^1)$ mg/l on both flood and ebb tide, with peaks of $O(10^2)$ mg/l (Figure 2). All models simulate this quite well during flood tide, but predict quite small SSCs during ebb. This is probably due to the simplified incorporation of erosion processes. Within-forest observations show SSC peaks of $O(10^{-1})$ mg/l on flood tide and minor resuspension during ebb tide (Figure 2). This is best simulated by the 3D-DPM model, simulating a 0.4 mg/l SSC peak during flood. The other two models predict SSCs within the forest of $O(1)$ mg/l during flood. None of the models predicts resuspension within the forest during ebb tide (Figure 4).

Cumulative net sediment deposition is presented in Figure 6 as well. The models simulate some deposition within the creek during high slack tide, but these deposits are eroded during the subsequent ebb tide. By the final retreat of the ebb tide from the creek, flow velocities and bed shear stresses drop again, causing a second deposition event. These deposits are presumably eroded at the onset of the next flood tide.

As for the SSCs, simulated deposition rates within the forest are diverging, but still in the same order of magnitude: $O(10^1)$ g/m^2. This is comparable to the field observations: 30-210 g/m^2 over two tidal cycles (Figure 1). At FC, a sediment deposition rate of 100 g/m^2/tide was observed. The results of the 3D-DPM run are quite low compared to these observations. Both 2DH models predict sediment deposition rates of one-half to one-third the rate observed at FC in the field site.

Figure 6 includes the sediment dynamics for the Manning vegetation model and the case with no vegetation. Without vegetation, SSCs in the forest are much greater due to higher flow velocities. Moreover, increased ebb tidal velocities cause erosion within the forest, feeding the ebb tidal SSC peak within the creek. These processes are reflected in increased deposition and erosion rates throughout the area, but
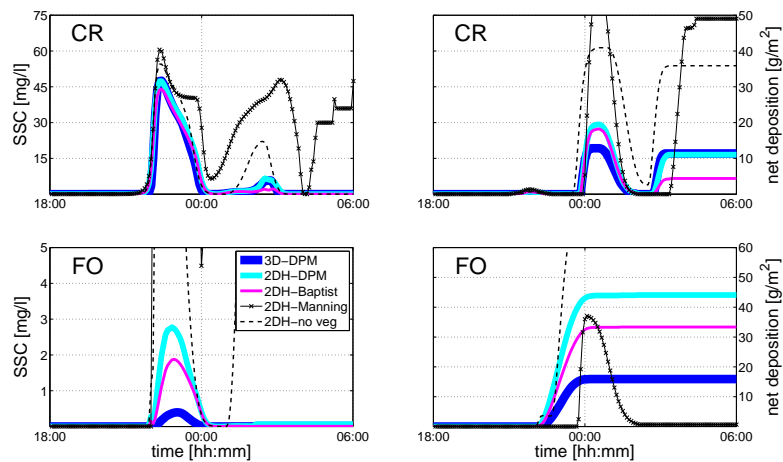

Figure 6. Simulated suspended sediment concentrations and cumulative deposition rates for points located within the creek (CR) and in the forest (FO). Results are from the same models as in Figure 4.

counter-intuitively give rise to a greater net deposition at FO than the vegetated model runs. This is due to the concentrated sediment deposition on the banks along the creek when vegetation is present. Without vegetation the sediment is transported further onto the intertidal flat, to FO, where deposition is enhanced. Total net sediment deposition throughout the area is greater with vegetation though ($2.1 \cdot 10^4$ and $2.8 \cdot 10^4$ kg for the non-vegetated and the 3DH-DPM runs, respectively). As stated before, the increased bed roughness of the Manning vegetation representation exaggerates bed shear stresses. Hence SSCs remain high, while deposition only occurs during slack high tide and erosion prevails throughout the area during ebb tide.

3.4. *Model sensitivity*

Model results presented so far are based on a single set of parameters (Table 1). However, conditions in the field are variable (Table 1) and parameters such as bed roughness and sediment characteristics introduce uncertainty in the model predictions. Moreover, horizontal viscosity and diffusivity are not readily obtained from the field. Hence we check the model's sensitivity to changes in these parameters. The fast – but according to the above results accurate – 2DH-DPM model was deployed for this sensitivity analysis.

Focusing on hydrodynamics, two uncertain parameters are relevant: viscosity v_H and bed roughness C_b. Ranges of these parameters were based on standard settings, grid size (section 2.5) and previous studies (e.g. Wolanski et al., 1990; Furukawa et al., 1997) respectively. For either increasing viscosity or increasing bed roughness, flow velocities are decreasing in the creek, while increasing in the forest (Table 2). With the highest viscosity or bed roughness values, flow reversal at high slack tide collapses, as opposed to the results in Figure 5. At the lower half of both ranges, model results become insensitive to these parameters.

Regarding sediment dynamics, the number of uncertain parameters increases (Table 2). Viscosity only shows minor impacts on simulated SSC's and deposition rates, while increasing bed roughness inherently affects these predictions. The greater bed shear stresses induce higher SSCs and reduced deposition, except for the forest, where the increased SSC enhances local deposition rates.

Critical bed shear stresses are hardly affecting sediment dynamics (Table 2), probably because of the limited range of variation. On the other hand, model predictions appear rather sensitive to the settling velocity (Table 2). Sediment transport throughout the forest diminishes substantially for increasing settling velocities, resulting in up to 14 times lower SSCs and net deposition reduced to one-third over the applied parameter range. Sediment dynamics within the creek are hardly affected, due to the greater velocities.

The erosion parameter is a poorly documented constant. It's standard value in Delft3D-FLOW is 10^{-4} kg/m^2/s, whereas data from literature suggest $M=10^{-3}$-10^0 kg/m^2/s (Van Rijn, 2006). Sediment dynamics within the forest are not significantly affected by this erosion parameter. In the creek, SSCs show increased fluctuations and sediments deposited at slack tide are removed faster on ebb tide for increased values of

Table 2: Sensitivity analysis of the 2DH-DPM model: parameter ranges are presented along with their impact on characteristic hydrodynamics and sediment dynamics (n.i. = no impact).

Parameter	Parameter range	Creek (CR)					Forest (FO)				
		$\bar{u}_{max}$ [m/s]		SSC_{max} [mg/l]		ND_{max} [g/m^2]	$\bar{u}_{max}$ [m/s]		SSC_{max} [mg/l]		ND_{max} [g/m^2]
		flood	ebb	flood	ebb		flood	ebb	flood	ebb	
v_H [m^2/s]	10^{-2}	0.63	-0.74	48	6	21	0.07	-0.09	2.7	0.04	45
	10^0	0.51	-0.67	45	12	25	0.10	-0.13	4.0	0.82	49
C_b [n]	0.01	0.68	-0.82	33	110	32	0.07	-0.09	1.4	0.00	24
	0.04	0.50	-0.59	54	1.2	18	0.09	-0.11	42	50	49
τ_{cr} [N/m^2]	0.10	n.i.	n.i.	51	10	18	n.i.	n.i.	3.1	0.13	47
	0.15	n.i.	n.i.	46	5.3	20	n.i.	n.i.	2.7	0.04	42
w_s [m/s]	$1 \cdot 10^{-3}$	n.i.	n.i.	46	6.1	22	n.i.	n.i.	14	0.28	71
	$7 \cdot 10^{-3}$	n.i.	n.i.	47	6.9	15	n.i.	n.i.	1.0	0.03	25
M [kg/m^2/s]	10^0	n.i.	n.i.	122	90	19	n.i.	n.i.	2.3	0.19	42
	10^{-4}	n.i.	n.i.	34	0.17	20	n.i.	n.i.	2.3	0.00	38
D_H [m^2/s]	10^{-1}	n.i.	n.i.	53	18	70	n.i.	n.i.	0.36	0.00	4.1
	10^1	n.i.	n.i.	23	0.55	3.2	n.i.	n.i.	7.3	0.15	104

this parameter (Table 2). At the high end of the erosion parameter's range, modeled SSCs become very variable (compared to the field data) while at the low end, sediment deposits are not removed from the creek during ebb tide, inducing ongoing deposition even within the creek.

Horizontal diffusivity, when lowered too much, generates the same effect as the increased erosion parameter (Table 2). On the contrary, with this parameter's standard value in Delft3D-FLOW (i.e. 10 m^2/s), sediment dynamics within the forest are suppressed substantially and become much lower than observed.

3.5. *Model calibration*

Without calibration, the hydrodynamics simulated by the 3D-DPM model and both 2DH models show good agreement when applying exactly the same parameter set. Moreover, simulated hydrodynamics compare favorably with field data for the applied viscosity and bed roughness (Table 1). The sensitivity analysis has learnt that changes to these parameters would reduce model performance in case of increases of these values, while a lowering would not induce significant changes (compare Table 2 and Figure 4).

Sediment dynamics showed quite a large variability between the models (Figure 6) and were not yet fully representing field observations. The occurrence of deposition and erosion are predicted well, but within the forest the magnitude of SSCs and net deposition do not resemble field observations (section 3.3). Model calibration is required to get the models to simulate correct SSCs and net deposition rates. From the sensitivity analysis it is found that the settling velocity is the best suitable parameter for this calibration's aim, i.e. adjusting the magnitude of SSC peaks and the cumulative deposition.

Previously, the 3D-DPM model was found to simulate field observations best, except for the rather low deposition rates at FO (16 g/m^2). This was adjusted by lowering the settling velocity to 2 mm/s, increasing the net deposition at FO (49 g/m^2) to resemble field data (Figure 2), but at the cost of overpredicting the SSC. However, SSC observations from the field are less accurate than deposition rates (Horstman, 2012).

The 2DH models were calibrated against the 3D-DPM model. The latter, resolving physical processes along the vertical, simulates tidal scale dynamics most accurately. Both 2DH models were calibrated in the sediment's settling velocity. Model runs deploying the range of settling velocities calculated from the field data (Table 1) were compared against the calibrated 3D-DPM model. Time averaged RMSE values are calculated for the entire model area, quantifying deviations between the predictions by the 2DH and the 3D-DPM models. For both 2DH models a settling velocity of 3 mm/s gives best agreement. Sediment dynamics predicted by the 2DH-DPM model agree best with the 3D simulation (RMSE(SSC)=0.47 and 0.69 mg/l; RMSE(ND)=2.9 and 7.3 g/m^2 for the 2DH-DPM and 2DH-Baptist models, respectively).

Figure 7 shows the resulting sediment dynamics after this basic calibration. Sediment dynamics within the creek basically remain unchanged. Only the deposition during high slack tide predicted by the 3D-DPM model is slightly increased and shows better agreement with the field observations. Within the forest, differences in predictions of SSCs are reduced, as are the simulated deposition rates. Better agreement of the model predictions at this specific location could have been obtained by calibrating the models for this position. However, a site specific calibration is of little value when comparing global model performance.
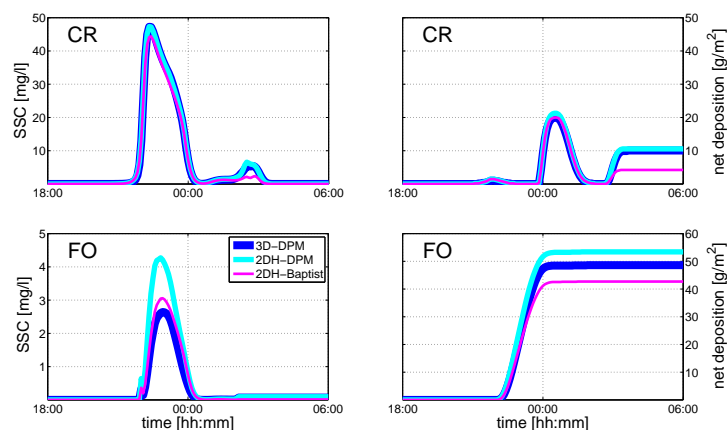

Figure 7. Adjusted model predictions after calibration of each model in the sediment settling velocity.

4. Discussion

The modeling efforts in this study concern tidal scale hydro- and sediment dynamics. Erosion is taken into account in a basic manner by simulating the erosion of sediments that have been deposited during the same tidal cycle. This is an extension to existing tidal marsh models simulating tidal-scale dynamics that only take account of sediment deposition while disregarding erosion (e.g. Temmerman et al., 2005). This means that sediments deposited within the creeks during high slack tide cannot be eroded on the subsequent ebb tide in Temmerman et al.'s model. However, self-scouring of tidal creeks is an essential mechanism in mangrove areas (e.g. Mazda et al., 1995). This is corroborated by the double peaks observed in the tidal SSC plots for the field site, showing within-creek SSC maxima during both flood and ebb (Figure 2). The models presented in the current paper (section 3.3) simulate these observations quite well (e.g. Figure 7). Still, model performance in predicting SSCs and erosion during ebb tide is limited as (long-term) morphodynamics are not fully taken into account. These require more advanced modeling of e.g. erosion processes and sediment compaction (c.f. Fagherazzi et al., 2012), which are beyond the scope of this study.

Spatial changes of fluxes due to (changes in) the vegetation's porosity are mostly considered negligible in the present models. The DPM vegetation representation was developed initially for 1DV conditions and has been implemented in Delft3D-FLOW as such (section 2.1). Only vertical momentum exchange, vertical diffusion of turbulent kinetic energy and vertical diffusion of turbulent energy dissipation are considered to depend significantly on the vegetation porosity (Baptist, 2005). However, horizontal momentum exchange and horizontal diffusion of turbulent properties may also play a role in water flowing through vegetation fields such as the creeks in our case study (e.g. Nepf, 2012).

Additionally, an inherent disadvantage of the 2DH models is that all vertical components of the physics guiding hydro- and sediment dynamics in the vegetated intertidal areas remain unresolved. Hence, it is impossible to study these processes, e.g. turbulence or depth-variation in velocities, in detail.

The previous assumptions are all adding to the simplicity and speed of the model simulations, especially for the 2DH models. Nevertheless, on a conceptual level, either of the models is capable of reproducing tidal-scale hydro- and sediment dynamics observed in the field. While model accuracy is found comparable – with the 2DH-DPM model best resembling the 3D model – model efficiency is greater for the 2DH models. One model simulation (covering 1.5 tidal cycle) only takes 7-10 minutes with the 2DH models while running the full 3D model takes about 10 times as long (1:15 h). The lower computational cost of the 2DH models facilitate sensitivity analyses such as presented in this study, but also when investigating e.g. the impact of vegetation thinning or removal.

The greater efficiency of the 2DH models will be of great use in future simulations of the tidal dynamics for the field site, where the irregular topography asks for a significant increase in grid size resolution. Finally, further model extensions to account for the long-term development of coastal mangroves, requiring e.g. the implementation of morphodynamics and long-term simulations, will further increase model demands. The efficiency of the 2DH model will enhance the feasibility of these extensions.

5. Conclusions

All models presented in this study, either 3D or 2DH, predict tidal hydro- and sediment dynamics in a mangrove creek catchment in accordance with field observations. For the schematized study area, only minor calibration efforts were needed to obtain comparable simulation results from each of the models. Best agreement was obtained between the 3D-DPM and 2DH-DPM models. Notwithstanding the fact that the 2DH models cannot account for the depth-variability in the vegetation, the 2DH-DPM model predicts tidal hydro- and sediment dynamics that are accurately resembling the 3D-DPM predictions for the presented study area. The 2DH-Baptist model slightly underpredicts the bed shear stresses within the forest, giving rise to deviations in predicted sediment dynamics, due to the simulation of the vegetation effects through an artificial bed roughness term. The reduction of the process resolution in the 2DH models comes with a significant increase in model efficiency. For our model area, which is small in terms of grid cells, and a 3D model with only 10 layers, the 2DH-DPM model was up to 10 times faster than the full 3D-DPM model. This reduction of calculation times will be of great use for future simulations of the tidal dynamics at the field site and for further model extensions to simulate long-term morphodynamics in mangroves.

Acknowledgements

References

Baptist, M.J., 2005. *Modelling floodplain biogeomorphology*. Delft University of Technology, Delft: 213 pp.

Baptist, M.J., Babovic, V., Rodríguez Uthurburu, J., Keijzer, M., Uittenbogaard, R.E., Mynett, A. and Verwey, A., 2007. On inducing equations for vegetation resistance. *Journal of Hydraulic Research*, 45(4): 435-450.

Bouma, T.J., Van Duren, L.A., Temmerman, S., Claverie, T., Blanco-Garcia, A., Ysebaert, T. and Herman, P.M.J., 2007. Spatial flow and sedimentation patterns within patches of epibenthic structures: Combining field, flume and modelling experiments. *Continental Shelf Research*, 27: 1020-1045.

Deltares, 2012. *User manual Delft3D-FLOW*, Deltares, Delft: 676 pp.

Fagherazzi, S., Kirwan, M.L., Mudd, S.M., Guntenspergen, G.R., Temmerman, S., D'Alpaos, A., Van De Koppel, J., Rybczyk, J.M., Reyes, E., Craft, C. and Clough, J., 2012. Numerical models of salt marsh evolution: Ecological, geomorphic, and climatic factors. *Reviews of Geophysics*, 50(RG1002).

Furukawa, K., Wolanski, E. and Mueller, H., 1997. Currents and sediment transport in mangrove forests. *Estuarine Coastal and Shelf Science*, 44(3): 301-310.

Horstman, E.M., 2012. *Data report: Field campaign Trang, Thailand; November 2010 - May 2011*, University of Twente, Enschede, The Netherlands.

Horstman, E.M., Dohmen-Janssen, C.M. and Hulscher, S.J.M.H., subm. Flow-routing in mangrove forests; field data obtained in Trang, Thailand. *Continental Shelf Research*.

Kobashi, D. and Mazda, Y., 2005. Tidal Flow in Riverine-Type Mangroves. *Wetlands Ecology and Management*, 13(6): 615-619.

Mazda, Y., Kanazawa, N. and Wolanski, E., 1995. Tidal asymmetry in mangrove creeks. *Hydrobiologia*, 295(1): 51-58.

Mazda, Y., Kobashi, D. and Okada, S., 2005. Tidal-Scale Hydrodynamics within Mangrove Swamps. *Wetlands Ecology and Management*, 13(6): 647-655.

Nepf, H.M., 2012. Hydrodynamics of vegetated channels. *Journal of Hydraulic Research*, 50(3): 262-279.

Temmerman, S., Bouma, T.J., Govers, G., Wang, Z.B., De Vries, M.B. and Herman, P.M.J., 2005. Impact of vegetation on flow routing and sedimentation patterns: Three-dimensional modeling for a tidal marsh. *Journal of Geophysical Research*, 110(F04019): 18.

Uittenbogaard, R.E., 2003. Modelling turbulence in vegetated aquatic flows. *International Workshop on RIParian FORest Vegetated Channels: Hydraulic, Morphological and Ecological Aspects*, Trento, Italy.

Van Rijn, L.C., 2006. *Principles of sediment transport in rivers, estuaries and coastal seas, part II*. Aqua Publications, Amsterdam.

Van Santen, P., Augustinus, P.G.E.F., Janssen-Stelder, B.M., Quartel, S. and Tri, N.H., 2007. Sedimentation in an estuarine mangrove system. *Journal of Asian Earth Sciences*, 29(4): 566-575.

Vo-Luong, H.P. and Massel, S.R., 2006. Experiments on wave motion and suspended sediment concentration at Nang Hai, Can Gio mangrove forest, Southern Vietnam. *Oceanologia*, 48(1): 23-40.

Wolanski, E., Mazda, Y., King, B. and Gay, S., 1990. Dynamics, flushing and trapping in Hinchinbrook channel, a giant mangrove swamp, Australia. *Estuarine Coastal and Shelf Science*, 31(5): 555-579.

Wolanski, E., Spagnol, S. and Ayukai, T., 1999. Field and model studies of the fate of particulate carbon in mangrove-fringed Hinchinbrook Channel, Australia. *Mangroves and Salt Marshes*, 2(4): 205-221.

Wu, Y., Falconer, R.A. and Struve, J., 2001. Mathematical modelling of tidal currents in mangrove forests. *Environmental Modelling & Software*, 16(1): 19-29.